Probing light emission from quantum wells within a single nanorod

Jochen Bruckbauer[1]**, Paul R Edwards**[1]**, Jie Bai**[2]**, Tao Wang**[2] **and Robert W Martin**[1]

[1] Department of Physics, SUPA, University of Strathclyde, Glasgow G4 0NG, UK
[2] Department of Electronic and Electrical Engineering, University of Sheffield, Sheffield S1 3JD, UK

E-mail: r.w.martin@strath.ac.uk

Abstract

Significant improvements in the efficiency of optoelectronic devices can result from the exploitation of nanostructures. These require optimal nanocharacterization techniques to fully understand and improve their performance. In this study we employ room temperature cathodoluminescence hyperspectral imaging to probe single GaN-based nanorods containing multiple quantum wells (MQWs) with a simultaneous combination of very high spatial and spectral resolution. We have investigated the strain state and carrier transport in the vicinity of the MQWs, demonstrating the high efficiencies resulting from reduced electric fields. Power-dependent photoluminescence spectroscopy of arrays of these nanorods confirms that their fabrication results in partial strain relaxation in the MQWs. Our technique allows us to interrogate the structures on a sufficiently small length scale to be able to extract the important information.

(Some figures may appear in colour only in the online journal)

1. Introduction

The rapid development of optoelectronic devices based on group III-nitride semiconductors in the last two decades has demonstrated their considerable potential for applications such as advanced solid-state lighting (SSL) [1, 2]. Light-emitting diodes (LEDs) using InGaN/GaN multiple quantum wells (MQWs) as their active region already exhibit excellent optical properties and are commercially available. However, the overall efficiencies of the devices still need to be improved and the fabrication costs lowered to enhance the large-scale commercialization of SSL [3, 4]. Due to the spontaneous and strain-induced piezoelectric polarizations along the c-direction, strong internal electric fields are induced [5]. These produce the quantum-confined Stark effect (QCSE), which redshifts the emission energy and decreases the emission intensity. Furthermore, the light extraction efficiency from the active region of the semiconductor is reduced by total internal reflection at the semiconductor–air interface. The use of semi-polar and non-polar planes offers one route to reducing the influence of the QCSE [6, 7]. Nanostructures, such as nanorods or nanowires, are reported to have enhanced performance due to additional quantum confinement, a reduction in the QCSE due to strain relaxation, and an improvement in light extraction [8–10]. Detailed investigation of the processes controlling the light emission from nanorods is still required to further understand the impact of strain and carrier transport within them.

We investigate the optical behaviour of individual, isolated GaN nanorods containing multiple InGaN quantum wells using cathodoluminescence (CL) hyperspectral imaging, and of nanorod arrays using photoluminescence (PL) spectroscopy. In contrast to other studies, the *simultaneous combination* of high spatial and spectral resolution provided by the CL technique makes it possible to obtain useful information from a single isolated nanostructure on a length scale approaching 10 nm [11, 12]. Conventional CL imaging records either the total spectrally integrated intensity (panchromatic) or the intensity distribution at a fixed

wavelength (monochromatic). By contrast, CL *hyperspectral imaging* is a more powerful technique in which an entire luminescence spectrum is recorded at each pixel in an image created by a scanning electron beam [13, 14]. The result is a multi-dimensional data set allowing the maximum information to be extracted from variations in luminescence spectra across the sample. Conventional CL mapping has been used for various kinds of nanorod structures fabricated from the group III-nitride system, e.g. GaN nanorods of various diameters, InGaN/GaN pedestal nanorods, core–shell InGaN/GaN nanorods or GaN nanorods containing an InGaN single quantum well [8, 15–18]. There have also been a few reports of in-depth spot-mode CL investigations of ZnO nanorods [19, 20]. The emphasis in this study is on *simultaneous combination* of high spatial and spectral resolution, with most previous reports employing pan-/monochromatic CL imaging or spot-mode CL.

2. Experimental section

The nanorods in this study were fabricated from planar In-GaN/GaN MQW samples, grown by metal-organic chemical vapour deposition, using a high-temperature AlN buffer layer and (0001)-orientated sapphire substrate [21]. The MQW structure consisted of five 3 nm thick InGaN wells and 10 nm thick GaN barriers, deposited on a nominally 1 μm thick GaN template and was completed by a GaN capping layer of nominal thickness 45 nm. High-resolution x-ray diffraction (HRXRD) yielded an InN content of 14% for the InGaN wells. We fabricated the nanorods using a self-assembled etch mask built from nickel droplets, produced by annealing a thin layer of Ni above a protective SiO_2 film [22]. A standard reactive ion etching process was used to create SiO_2 nanorods and the sample was then etched in an inductively coupled plasma until parts of the thick GaN template were exposed. Finally, the etch mask was removed. We characterized the surface morphology of the nanorods using a scanning electron microscope, to which a customized CL system has been added [11, 23].

The sample holder is tilted by 45° with respect to the electron beam as seen in figure 1(b). The light is collected by a reflecting objective with its optical axis perpendicular to the electron beam and is detected using a spectrograph with a cooled electron multiplying charge-coupled device. The spectral resolution is approximately 0.2 nm. We used an electron beam acceleration voltage of 5 kV and beam currents of up to 10 nA. CL spectra were recorded at each pixel and then fitted with Voigt and/or Gaussian functions to create two-dimensional maps, which plot each different fitting parameter (e.g. energy peak position and peak intensity) against position on the sample.

Monte Carlo simulation indicates that, under a 5 kV electron beam normally incident on a GaN surface, 90% of carriers are generated within a region of radius approximately 62 nm. The volume from which the CL is generated is further enlarged by the carrier diffusion length. However, our data demonstrate useful information on a length scale approaching 10 nm, showing that combination of the nanostructure and
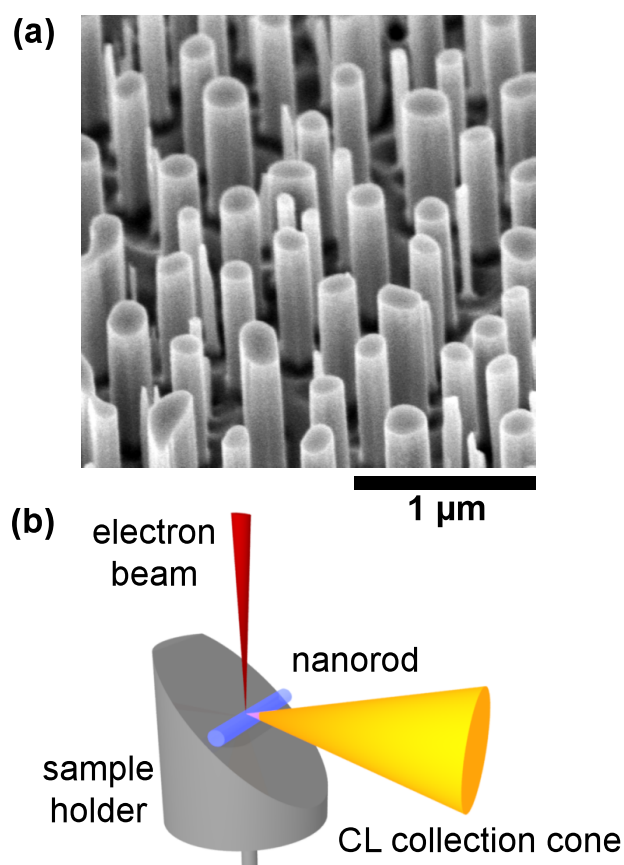
Figure 1. (a) Typical SE image of the nanorod array after the etch process, showing nanorods with diameters in the range of 100–300 nm. (b) Schematic diagram of the CL measurement geometry for a single nanorod showing the sample on a 45° tilted holder.

spectral mapping allows greater 'resolution' than normally expected [12].

In order to probe single nanorods, we detached the nanorods from the original array and dispersed them in a solution of acetone, which was then deposited on a clean piece of silicon wafer and left to evaporate. Secondary electron (SE) imaging was then performed on this sample to locate isolated nanorods for subsequent recording of CL hyperspectral images.

PL measurements were carried out in a closed-cycle helium cryostat using a 405 nm laser diode as the excitation source, chosen to selectively excite the InGaN quantum wells (QWs) and not the bulk GaN. The maximum laser power at the sample was approximately 44 mW. Neutral density filters were used to reduce the laser intensity for power-dependent PL.

3. Results and discussion

A typical SE micrograph of the nanorod array after the etching procedure is shown in figure 1(a), where the sample is viewed at 45° (figure 1(b)). The nanorods have diameters ranging from 100 to 300 nm, an average length of 900 nm and a density in the mid 10^8 cm^{-2} regime.

(a)

SEM

500 nm

(b)

CL

16000

14000

12000

10000

Integrated intensity (counts)

500 nm

(c)
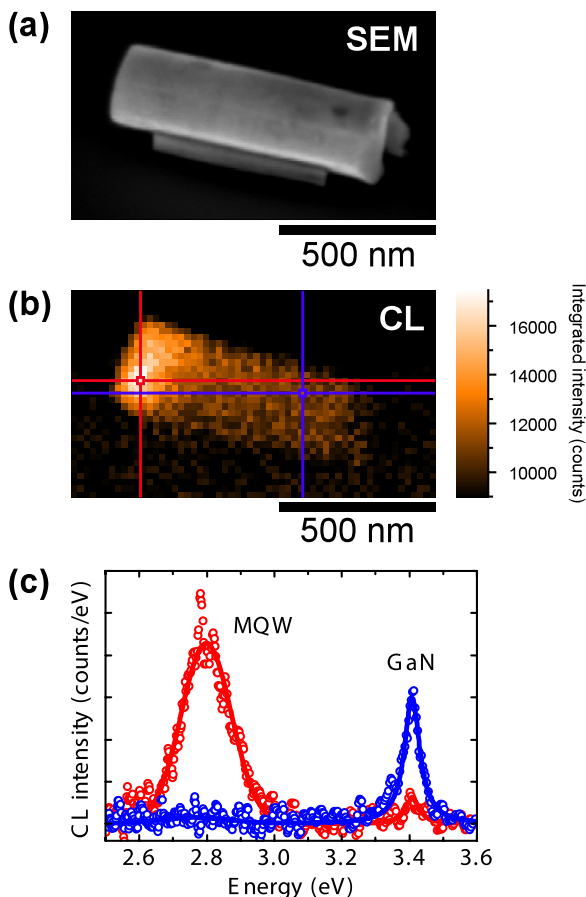
Figure 2. (a) SE electron image of an isolated nanorod with a 250 nm diameter on a silicon substrate. (b) Corresponding panchromatic CL map at room temperature showing the total integrated CL intensity. (c) Representative CL spectra with fits of the MQW and GaN emission taken from two pixels of the hyperspectral image indicated by the two crosshairs in (b).

For the optical investigation of an individual, isolated nanorod, we separated the nanorods from the GaN template and deposited them on a clean silicon wafer. A typical SE micrograph after isolation of a nanorod with a 250 nm diameter is shown in figure 2(a). The left-hand side corresponds to the top of the nanorod. We acquired the room temperature CL hyperspectral image of this nanorod using an acceleration voltage of 5 kV, a beam current of about 6 nA, a step size of 20 nm and an exposure time of 20 ms/spectrum. Figure 2(b) displays the integrated CL intensity map. This map is equivalent to a conventionally acquired panchromatic CL image and clearly shows a region of higher intensity at the top of the nanorods, corresponding to the location of the QW stack. Figure 2(c) shows representative CL spectra from the hyperspectral CL image, with one from a pixel within the area with high intensity (i.e. quantum well emission) and the second from further down the rod (showing GaN emission). Similar observations of a single quantum well nanorod have been reported at lower spatial resolution using microphotoluminescence [24].

Each spectrum in the hyperspectral image consists of a peak originating from the GaN band edge emission,

near 3.41 eV, and one from the MQW emission, near 2.8 eV. For a more detailed analysis of the hyperspectral image, we numerically fitted these peaks in each spectrum using Voigt and Gauss functions for the GaN and MQW peaks, respectively. The resulting CL energy and intensity maps of the GaN and MQW emission are reproduced in figures 3(a)–(d). To aid visualization we use the corresponding CL intensity maps as a mask to display only the area in the CL energy maps where the intensity exceeds the noise level.

The map of the GaN emission energy in figure 3(a) reveals a negligible energy shift along the axis of the nanorod, indicating that there is no variation in strain within the GaN region of the nanorod. The room temperature transition energy of the A-exciton in single-crystal GaN films occurs at 3.42 eV, which is close to the measured GaN band edge emission of 3.41 eV in the CL map [25]. The emission at the lower side of the nanorods is slightly redshifted, which is likely to be a result of self-absorption. The excitation and measurement geometry becomes very important in the case of three-dimensional structures. The nanorod in figure 2(a) lies horizontally on the 45° tilted sample holder; when the electron beam excites the 'uphill' side of the nanorod (corresponding to the lower side in the SE and CL images) the emitted light has to pass through the rod before reaching the detection optics as seen in figure 3(e). Stronger absorption of the emitted light by the GaN can therefore result in a small apparent narrowing and redshift. The influence of the geometry on the CL measurement is further described by Edwards *et al* [11].

The map of the MQW peak energy in figure 3(c) shows that there is no energy shift perpendicular to the axis of the nanorod, whereas a small redshift occurs along the growth direction. The MQW emission energy changes by approximately 18 meV over the width of the MQW region, as can be seen in figure 3(f), which shows an energy line scan through the MQW region along the nanorod axis. Such a redshift could arise through a number of different mechanisms. Variation in the emission energy *within the MQW region* itself would result, for example, from well-to-well differences in composition or thickness, or from a relaxation of the compressive strain along the growth axis. However, these effects are usually interrelated, and also influence the strength of the QCSE, making it difficult to determine which one dominates. *Outside the MQW region*, however, these effects would not be expected to influence the emission energy at all, since a given pixel in the CL map corresponds to the region at which carriers are generated and not to the region where the radiative recombination occurs. Carriers generated outside the active region may diffuse to the nearest well, but the emission energy from the resultant recombination will not depend on the properties of the GaN at the point of the electron beam incidence. The dominant mechanism accounting for the blueshift in MQW emission as the beam scans towards the MQW region from the underlying GaN (from the right-hand side of the figure) is the screening of the internal electric field by the increasingly high density of e-beam-generated carriers. As the electron beam moves through the MQW stack towards the top of the nanorod the MQW peak energy is observed to redshift. An additional
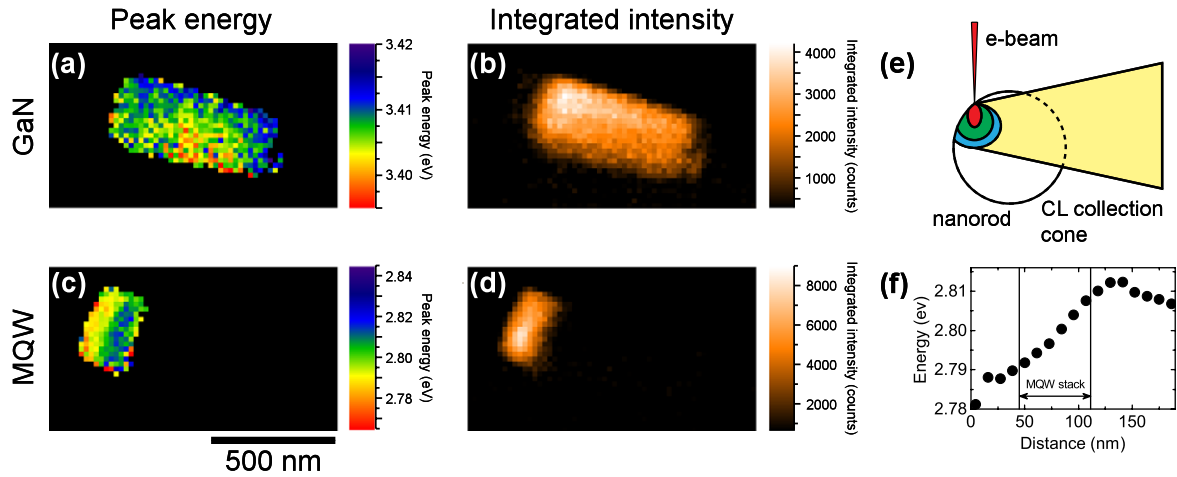
Figure 3. Room temperature CL maps gained by fitting the hyperspectral data set in figure 2(b) with Voigt and Gauss functions for the GaN and MQW emission peaks, respectively: (a) peak energy and (b) integrated intensity maps of the GaN band edge emission and (c) peak energy and (d) integrated intensity maps of the MQW emission. Using the spectral information gained by peak fitting it is possible to identify the spatial origin of the two peaks and map shifts in their energy. The MQW emission is located on the left-hand side corresponding to the top of the nanorod, whereas the GaN emission originates from the area below this region. The map of the GaN peak shows a negligible energy shift along the nanorod axis suggesting no variation in strain. However, the map of the MQW emission displays a small redshift towards the top surface of the nanorod. (e) Schematic diagram showing the influence of self-absorption. Light generated on the left-hand side of the rod has to pass through the nanorod to reach the detection optics. The excitation volume induced by the electron beam is also shown. (f) Line scan through the MQW emission energy map in (c) showing a small redshift along the axis towards the top of the nanorod.
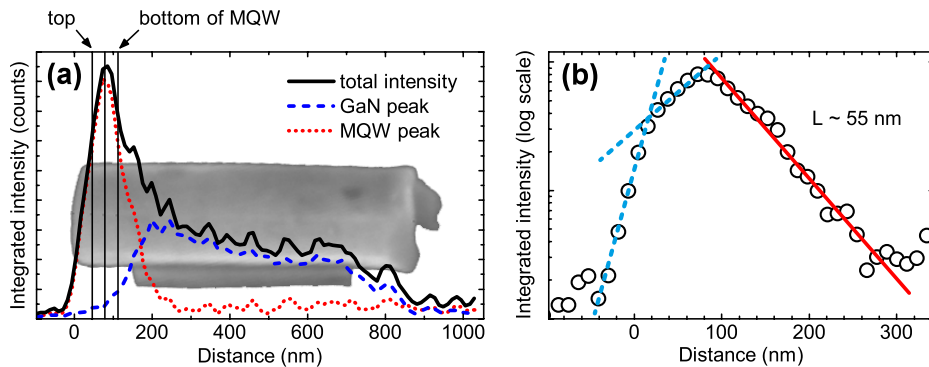
Figure 4. (a) Integrated intensity line scans of the MQW and GaN emission from the CL maps in figures 3(b) and (d) superimposed on the SE image of an isolated rod. The three vertical, parallel lines mark the top, centre and bottom of the QW stack on the nanorod as determined by x-ray diffraction. The maximum of the total intensity is in good agreement with the calculated centre of the MQW region. (b) Logarithmic intensity plot of the same line scan (red dotted line in (a)) through the QW stack. The red solid line is a fit to the simple one-dimensional diffusion equation for calculating the carrier diffusion length L at room temperature.

important factor is now the impact of the top surface of the nanorod, which is approximately 100 nm from the deepest QW and has come within the excitation volume. Diffusion of e-beam-generated carriers to trap states at the top surface, and the reduced generation volume, combine to reduce the screening and produce the redshift towards the top of the rod.

We next plot line scans of the integrated intensities of the MQW and GaN emission along the nanorod axis, as shown in figure 4(a), to further investigate the emission behaviour of the MQW structure. To identify the spatial origin of the luminescence the line scans are superimposed on the SE image of the isolated nanorod on the same scale. Using HRXRD on the as-grown wafer we estimate the centre of the MQW structure to be approximately 77 nm below the top of the rod, which is matched to the maximum of the MQW emission intensity. The intensity profile is in

good agreement with the SE image, i.e. the length of the nanorod. However, the bottom of the rod does not show much light emission, which might be caused by structural damage sustained during detachment from the GaN template. At the other end the intensity drops down rapidly due to the electron beam scanning over the top edge. A closer look at the MQW emission intensity reveals three different slopes in the vicinity of the maximum as seen in the logarithmic plot of the integrated MQW intensity in figure 4(b). We relate the steep drop at the top end of the nanorod to a combination of the limit of the sample and surface recombination. The second region on the left side of the maximum, which has a shallower slope, is related to carrier distribution within the wells, as discussed below. There is only one slope on the lower side, which is similar to the second one, but continues further into the GaN part of the rod. Carriers generated in

the thick GaN layer below the MQWs can reach the wells from areas further away and contribute to the MQW intensity. This exponential decay of the intensity suggests that a simple one-dimensional diffusion equation of the form $I \propto e^{-\frac{x}{L}}$ can be used to fit the CL intensity. The calculated carrier diffusion length of $L \approx 55$ nm for this 250 nm wide nanorod matches well with the lower limit of the diffusion length of 50–60 nm previously obtained from InGaN/GaN layers [26, 27]. It should be mentioned, however, that these diffusion lengths were estimated from dark spots (non-radiative recombination centres) in plan-view panchromatic CL images and measures in-plane diffusion in either material, whereas here L is calculated from the intensity profile along the [0001] axis of the nanorod. The slopes on either side of the intensity maximum are very similar, as it makes no difference on which side the excitation occurs. This intensity distribution will be the result of the convolution of the carrier generation function and the quantum well profile, coupled with the subsequent diffusion of the carriers. Alternative methods using monochromatic CL intensity profiles and/or spotspectra were used to estimate the diffusion lengths of 100 and 200 nm at low temperature (5 K) in ZnMgO and ZnO nanowires [28, 29].

To shed light on the strain situation, we investigated low-temperature PL spectra from the as-grown and nanorod array samples, as shown for the highest laser power of 44 mW in figure 5(a). The rows of data points above the two peaks correspond to measurements from different positions several millimetres apart on the sample and indicate the extent of a slight variation in the emission energy across the surface. In addition, two longitudinal optical (LO) phonon replicas are resolved. We observe notable differences between the spectra for the nanorod and the as-grown sample with the energy blueshifted by about 12 nm (70 meV) and the optical linewidths of the main emission peaks (zero-phonon line) decreased by about 20 meV.

A characteristic of (0001)-oriented InGaN/GaN quantum well structures is the presence of strain-induced internal electric fields along the growth direction leading to the well-known QCSE, which shift the emission peak towards lower energies. The observed blueshift is likely to be caused by a reduction of the piezoelectric polarization, which shifts the band profile back towards the flat-band condition [30, 31]. In this case the blueshift can be interpreted as a relaxation of strain in the MQW structures after the formation of the nanorod arrays. Pseudomorphic grown InGaN wells on GaN, however, are compressively strained, which increases the band gap and hence the emission energy compared to the unstrained case. Relaxation of the compressive strain would then result in a decrease of the emission energy. This indicates that the energy shift related to the reduction of the QCSE is stronger than the shift resulting from the reduction of the compressive strain. Fabrication of nanorods also decreased the optical linewidth of the nanorod emission, as seen in figure 5(a). With increasing piezoelectric fields the electron–hole wavefunction overlap decreases, which results in an inhomogeneous broadening of the linewidth [32]. The observed decrease in linewidth of the nanorods supports this finding of a reduced influence of the QCSE. The reduction of
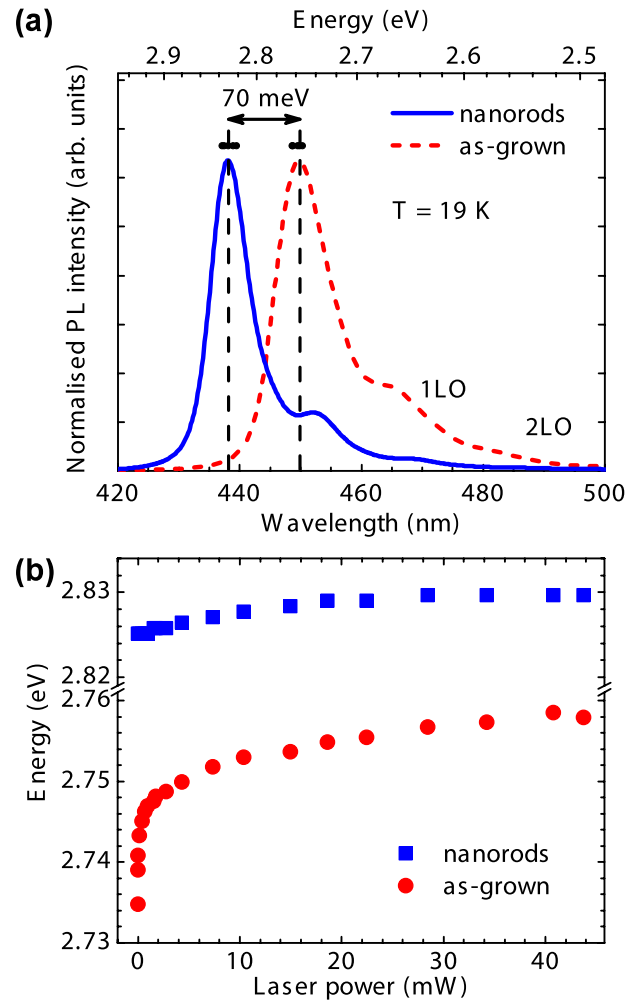
Figure 5. (a) Low-temperature photoluminescence spectra show a blueshift and linewidth narrowing of the emission peak of the nanorod compared to the as-grown sample. (b) Power-dependent PL of the as-grown sample compared to the nanorod sample displays a blueshift with increasing laser power. The different magnitude of this blueshift indicates a decrease of the internal electric fields, i.e. weaker QCSE, in the nanorod sample. The spectra were recorded at 19 K.

the piezoelectric field strength can be estimated to be about 0.23 MV cm^{-1} using the energy shift and the well width, which is comparable to results from similar nanorods, albeit of greater diameter, as reported by Chiu *et al* [30].

We also performed low-temperature power-dependent PL measurements on the as-grown and nanorod samples, as displayed in figure 5(b). Although both exhibit a blueshift with increasing laser power, the shift is stronger for the as-grown sample (23 meV) compared to the nanorod sample (5 meV). As mentioned above, the influence of the QCSE results in a redshift of the emission energy. With increasing laser power more charge carriers are excited in the wells and the internal electric fields are screened to a greater extent. As a result the emission energy increases with increasing excitation intensity. The difference in the strength of this blueshift further supports our argument concerning relaxation in the InGaN well layers, since before the fabrication of the nanorods the as-grown layer is heavily strained. Fabrication

of the nanorods relaxes the well material and as a result the QCSE is weaker. Therefore, the blueshift with increasing laser power is less pronounced in the nanorods than the as-grown sample. Compositional non-uniformity in the wafer as suggested by Keller *et al* [33] is a less likely explanation, as measurements on different positions on the sample display a smaller spread in energy than the energy shift between as-grown and nanorod samples as seen by the dots above the emission peak in figure 5(a). Related work has been reported for InGaN/GaN microdisks and tapered nanoposts [31, 34].

Reciprocal space map (RSM) measurements of similar nanorod structures with varying InN compositions by Wang *et al* [35] further support the above conclusion. An RSM of the as-grown layer showed that the InGaN MQWs were pseudomorphically grown on the GaN buffer layer, i.e. the MQW structure is under compressive strain. By contrast, an RSM of the nanorod sample displayed an increase of the in-plane lattice constant approaching the fully relaxed point. This sample had a higher InN composition than the sample discussed here and exhibited an 80% strain relaxation, whereas a sample with lower InN content was almost fully relaxed. Therefore, it is most likely that the observed blueshift of the nanorods compared to the as-grown sample in figure 5(a) is due to this partial strain relaxation in the MQW structure as provided by the RSM findings. A first study of blue LEDs employing these InGaN/GaN nanorods by Bai *et al* [22] showed enhanced emission and similar current–voltage characteristics compared with planar LEDs.

4. Conclusion

In summary, we have demonstrated highly spatially *and* spectrally resolved CL hyperspectral imaging of individual InGaN/GaN MQW nanorods using a scanning electron microscope. The absence of an energy shift in the emission from the GaN below the MQWs signifies that there is negligible strain variation along the rod axis in this layer. In contrast, the MQW emission energy changes by approximately 18 meV across the region containing the wells. A line scan through the MQW emission intensity showed a simple exponential behaviour, allowing us to estimate a carrier diffusion length in the GaN rod at room temperature. Power-dependent PL of the as-grown MQW and nanorod sample showed a smaller blueshift with increasing excitation power after nanorod fabrication. This is a strong indicator for partial strain relaxation in the MQW structure as a result of a reduction in the influence of the QCSE, as also suggested by RSM measurements using HRXRD. These results will have significant impact on the use of nanorods to improve optoelectronic devices such as white LEDs (i.e. blue LED chips coated with a phosphor) and violet/blue laser diodes. An increasing InN content enhances the piezoelectric polarization, which reduces the efficiency due to induced internal electric fields leading to the so-called 'green gap'. Since the polarization is dependent upon the crystal orientation, growth on semi- or non-polar planes reduces or eliminates these electric fields; however the substrates for growth are very expensive. We have presented an analysis of the strain relaxation in the nanorods confirming that they allow an alternative route to reduce the built-in electric fields, and thus offer a cheaper and easier path to the mass production of high performance, ultra-efficient LEDs. Our technique allows us to probe the light emission on a sufficiently small length scale to extract the relevant information.

Acknowledgments

References

[1] Nakamura S, Mukai T and Senoh M 1994 *Appl. Phys. Lett.* **64** 1687
[2] Steele R V 2007 *Nature Photon.* **1** 25
    Haitz R and Tsao J Y 2011 *Phys. Status Solidi* c **208** 17
[3] Schubert E F and Kim J K 2005 *Science* **308** 1274
[4] Wierer J J, David A and Megens M M 2009 *Nature Photon.* **3** 163
[5] Bernardini F, Fiorentini V and Vanderbilt D 1997 *Phys. Rev.* B **56** R10024
    Waltereit P, Brandt O, Trampert A, Grahn H T, Menniger J, Ramsteiner M, Reiche M and Ploog K H 2000 *Nature* **406** 865
[6] Ueda M, Kojima K, Funato M, Kawakami Y, Narukawa Y and Mukai T 2006 *Appl. Phys. Lett.* **89** 211907
[7] Chakraborty A, Haskell B A, Keller S, Speck J S, DenBaars S P, Nakamura S and Mishra U K 2004 *Appl. Phys. Lett.* **85** 5143
[8] Kim H-K, Kim D S, Kim D Y, Kang T W, Cho Y-H and Chung K S 2002 *Appl. Phys. Lett.* **81** 2193
[9] Yan R, Gargas D and Yang P 2009 *Nature Photon.* **3** 569
[10] Ramesh V, Kikuchi A, Kishino K, Funato M and Kawakami Y 2010 *J. Appl. Phys.* **107** 114303
[11] Edwards P R and Martin R W 2011 *Semicond. Sci. Technol.* **26** 064005
[12] Bruckbauer J, Edwards P R, Wang T and Martin R W 2011 *Appl. Phys. Lett.* **98** 141908
[13] Christen J, Grundmann M and Bimberg D 1991 *J. Vac. Sci. Technol.* B **9** 2358
[14] Martin R W, Edwards P R, O'Donnell K P, Dawson M D, Jeon C-W, Liu C, Rice G R and Watson I M 2004 *Phys. Status Solidi* a **201** 665
[15] Jahn U, Ristić J and Calleja E 2007 *Appl. Phys. Lett.* **90** 161117
[16] Seo H W, Tu L W, Lin Y T, Ho C Y, Chen Q W, Yuan L, Norman D P and Ho N J 2009 *Appl. Phys. Lett.* **94** 201907
[17] Bergbauer W *et al* 2010 *Nanotechnology* **21** 305201
[18] Kunert G *et al* 2011 *Nanotechnology* **22** 265202
[19] Pan N, Wang X, Li M, Li F and Hou J G 2007 *J. Phys. Chem.* C **111** 17265
[20] Schirra M, Reiser A, Prinz G M, Ladenburger A, Thonke K and Sauer R 2007 *J. Appl. Phys.* **101** 113509
[21] Bai J, Wang T, Comming P, Parbrook P J, David J P R and Cullis A G 2006 *J. Appl. Phys.* **99** 023513
[22] Bai J, Wang Q and Wang T 2012 *Phys. Status Solidi* a **209** 477
[23] Edwards P R, Sleith D, Wark A W and Martin R W 2011 *J. Phys. Chem.* C **115** 14031
[24] Holmes M J, Park Y S, Wang X, Chan C C S, Reid B P L, Kim H, Taylor R A, Warner J H and Luo J 2011 *Appl. Phys. Lett.* **98** 251908

[25] Shan W, Schmidt T J, Yang X H, Hwang S J, Song J J and Goldenberg B 1995 *Appl. Phys. Lett.* **66** 985

[26] Chichibu S, Wada K and Nakamura S 1997 *Appl. Phys. Lett.* **71** 2346

[27] Sugahara T, Sato H, Hao M, Naoi Y, Kurai S, Tottori S, Yamashita K, Nishino K, Romano L T and Sakai S 1998 *Japan. J. Appl. Phys.* **37** L398

[28] Yoo J, Yi G-C and Dang L S 2008 *Small* **4** 467

[29] Hwang J-S, Donatini F, Pernot J, Thierry R, Ferret P and Dang L S 2011 *Nanotechnology* **22** 475704

[30] Chiu C H *et al* 2007 *Nanotechnology* **18** 445201

[31] Dai L, Zhang B, Lin J Y and Jiang H X 2001 *J. Appl. Phys.* **89** 4951

[32] O'Donnell K P, Breitkopf T, Kalt H, der Stricht W V, Moerman I, Demeester P and Middleton P G 1997 *Appl. Phys. Lett.* **70** 1843

[33] Keller S *et al* 2006 *J. Appl. Phys.* **100** 054314

[34] Chen H-S, Yeh D-M, Lu Y-C, Chen C-Y, Huang C-F, Tang T-Y, Yang C C, Wu C-S and Chen C-D 2006 *Nanotechnology* **17** 1454

[35] Wang Q, Bai J, Gong Y P and Wang T 2011 *J. Phys.* D **44** 395102